Atmos. Chem. Phys., 23, 10697–10711, 2023
https://doi.org/10.5194/acp-23-10697-2023

Atmospheric Chemistry and Physics
Open Access
EGU

Research article

Enrichment of calcium in sea spray aerosol: insights from bulk measurements and individual particle analysis during the R/V *Xuelong* cruise in the summertime in Ross Sea, Antarctica

Bojiang Su[1,2], Xinhui Bi[1,3], Zhou Zhang[2,4], Yue Liang[5], Congbo Song[6], Tao Wang[1,2], Yaohao Hu[1,2], Lei Li[7], Zhen Zhou[7], Jinpei Yan[8], Xinming Wang[1,3], and Guohua Zhang[1,3]

[1]State Key Laboratory of Organic Geochemistry and Guangdong Provincial Key Laboratory of Environmental Protection and Resources Utilization, Guangzhou Institute of Geochemistry, Chinese Academy of Sciences, Guangzhou 510640, China
[2]University of Chinese Academy of Sciences, Beijing 100049, China
[3]Guangdong-Hong Kong-Macao Joint Laboratory for Environmental Pollution and Control, Guangzhou 510640, China
[4]State Key Laboratory of Isotope Geochemistry, Guangzhou Institute of Geochemistry, Chinese Academy of Sciences, Guangzhou 510640, China
[5]Department of Civil and Environmental Engineering, Faculty of Science and Technology, University of Macau, Taipa, Macau SAR, China
[6]National Centre for Atmospheric Science (NCAS), University of Manchester, Manchester, M13 9PL, UK
[7]Institute of Mass Spectrometry and Atmospheric Environment, Jinan University, Guangzhou 510632, China
[8]Key Laboratory of Global Change and Marine Atmospheric Chemistry, Third Institute of Oceanography, Ministry of Natural Resources, Xiamen 361005, China

Correspondence: Lei Li (lileishdx@163.com) and Guohua Zhang (zhanggh@gig.ac.cn)

Received: 23 February 2023 – Discussion started: 24 March 2023
Revised: 6 June 2023 – Accepted: 23 August 2023 – Published: 26 September 2023

Abstract. Although calcium is known to be enriched in sea spray aerosols (SSAs), the factors that affect its enrichment remain ambiguous. In this study, we examine how environmental factors affect the distribution of water-soluble calcium (Ca^{2+}) distribution in SSAs. We obtained our dataset from observations taken during the R/V *Xuelong* research cruise in the Ross Sea, Antarctica, from December 2017 to February 2018. Our observations showed that the enrichment of Ca^{2+} in aerosol samples was enhanced under specific conditions, including lower temperatures ($< -3.5\,°C$), lower wind speeds ($< 7\,m\,s^{-1}$), and the presence of sea ice. Our analysis of individual particle mass spectra revealed that a significant portion of calcium in SSAs was likely bound with organic matter (in the form of a single-particle type, OC-Ca, internally mixed organics with calcium). Our findings suggest that current estimations of Ca^{2+} enrichment based solely on water-soluble Ca^{2+} may be inaccurate. Our study is the first to observe a single-particle type dominated by calcium in the Antarctic atmosphere. Our findings suggest that future Antarctic atmospheric modeling should take into account the environmental behavior of individual OC-Ca particles. With the ongoing global warming and retreat of sea ice, it is essential to understand the mechanisms of calcium enrichment and the mixing state of individual particles to better comprehend the interactions between aerosols, clouds, and climate during the Antarctic summer.

Published by Copernicus Publications on behalf of the European Geosciences Union.

1 Introduction

Sea spray aerosols (SSAs) govern radiative forcing by directly scattering and absorbing solar radiation over the remote ocean (Murphy et al., 1998), and they affect the microphysical properties of marine clouds by serving as cloud condensation nuclei (CCN) and ice nuclei (IN) (Wilson et al., 2015; Brooks and Thornton, 2018; Willis et al., 2018). Calcium is one of the components of SSA, which can present as inorganic calcium (e.g., $CaCl_2$ and $CaSO_4$) (Chi et al., 2015) as well as organic calcium (i.e., Ca^{2+} can readily induce the gelation of organic matter, presenting as the most efficient gelling agent) (Carter-Fenk et al., 2021). Calcium enrichment and chemical signature can affect some physicochemical properties of SSAs such as alkalinity and hygroscopicity (Salter et al., 2016; Mukherjee et al., 2020), which is critical for understanding aerosol–cloud interactions over the remote marine boundary layer (Keene et al., 2007; Leck and Svensson, 2015; Bertram et al., 2018).

Several studies have demonstrated significant enrichment of calcium (Ca^{2+}) in SSAs compared to bulk seawater, as briefly summarized in Table S1 in the Supplement and documented by Keene et al. (2007), Hara et al. (2012), Cochran et al. (2016), Salter et al. (2016), Cravigan et al. (2020), and Mukherjee et al. (2020). For example, Hara et al. (2012) found that the Ca^{2+} enrichment of aerosol samples was sensitive to sea salt fractionation during the cold winter–spring season over the Antarctic coast. Leck and Svensson (2015) suggested that Ca^{2+} enrichment in SSAs is attributed to bubble bursts on sea ice leads over the Arctic area. Similarly, low-wind-driven bubble bursts were regarded as a major reason for the Ca^{2+} enrichment in SSAs during an Arctic cruise (Mukherjee et al., 2020). These results shed light on the Ca^{2+} enrichment process; however, our understanding of how environmental factors synergistically affect such enrichment processes remains unclear.

To date, a unified consensus on the chemical form of calcium to explain calcium enrichment in SSAs has not been reached. Two hypotheses have been proposed: (i) calcium enrichment is dominated by inorganic calcium, such as $CaCO_3$ and $CaCl_2$. Ca^{2+} is enriched close to the seawater surface in the form of ionic clusters (most probably with carbonate ions) (Salter et al., 2016). Another source of $CaCO_3$ is directly from calcareous shell debris (Keene et al., 2007). Through bubble bursts, both $CaCO_3$ and $CaCl_2$ along with sea salt can be emitted into the atmosphere. In addition, the sea salt fractionation by precipitation of ikaite ($CaCO_3 \cdot 6H_2O$) may contribute to calcium enrichment in aerosol during the freezing of sea ice (Hara et al., 2012). (ii) Calcium enrichment is attributed to organically complexed calcium. Ca^{2+} may bind with organic matter, which is relevant with marine microgels and/or coccolithophore phytoplankton scales, and can be emitted by bubble bursting (Oppo et al., 1999; Sievering, 2004; Leck and Svensson, 2015; Cochran et al., 2016; Kirpes et al., 2019; Mukherjee et al., 2020). The chemical form of calcium can determine its atmospheric role. Inorganic calcium may exhibit stronger aerosol alkalinity and hygroscopicity than organic calcium (Salter et al., 2016; Mukherjee et al., 2020). However, current estimations of calcium enrichment based solely on water-soluble Ca^{2+} may not precisely explain the calcium distribution in SSAs. This is because the amount of low water-soluble complexation of Ca^{2+} with organic matter (e.g., aged Ca^{2+}-assembled gel-like particles) (Orellana and Verdugo, 2003; Leck and Bigg, 2010; Russell et al., 2010; Orellana et al., 2011; Leck and Svensson, 2015) and insoluble Ca^{2+} in the form of calcareous shell debris or the like may not be considered. Thus, an alternative method, such as discerning the mixing state based on single-particle analysis, may provide unique insights into the chemical form of calcium and, thus, the mechanisms of calcium enrichment in SSAs.

As a part of the 34th Chinese Antarctic Research Expedition (CHINARE ANT34th), this study aimed to investigate the influencing factors and possible mechanisms of calcium enrichment in SSAs through R/V *Xuelong* cruise observation campaigns over the Ross Sea, Antarctica. An in situ gas and aerosol composition monitoring system (IGAC) was employed to determine the extent of Ca^{2+} enrichment in SSAs. Single-particle aerosol mass spectrometry (SPAMS) was utilized to measure the size and chemical signature (i.e., mixing state) of individual calcareous particles. We first investigated the impact of environmental factors such as ambient temperature, wind speed, sea ice fraction, chlorophyll *a* concentration, and back trajectory coverage on Ca^{2+} enrichment in SSAs. Then, the mechanisms of calcium enrichment in SSAs were inferred according to the mixing state of individual calcareous particles.

2 Methodology

2.1 The R/V *Xuelong* cruise and observation regions

Our study focused on the Ross Sea region of Antarctica (50 to 78° S, 160 to 185° E) (Fig. 1), where we conducted two separate observation campaigns aboard the R/V *Xuelong*. During the observations, this region was relatively isolated from the impact of long-range transport of anthropogenic aerosols and experienced sea ice retreat (Yan et al., 2020a).

The first observation campaign (leg I) took place from 2–20 December 2017, during the sea ice period. The second campaign (leg II) was conducted from 13 January to 14 February 2018, during the period without sea ice. The sampling design for legs I and II aimed to investigate how changing environmental factors affect the enrichment extent of calcium and the characteristics of individual particles.

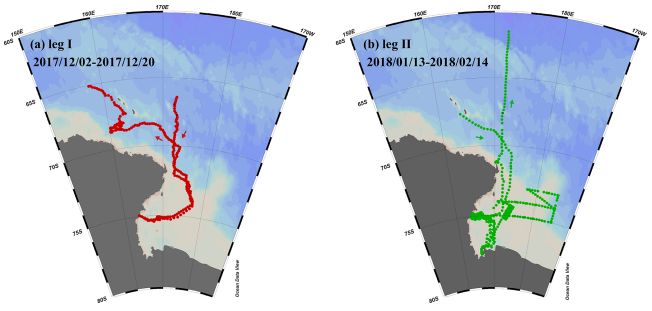

Figure 1. Observation campaigns through R/V *Xuelong* in the Ross Sea, Antarctic. **(a)** Leg I took place from 2–20 December 2017. **(b)** Leg II was conducted from 13 January to 14 February 2018.

2.2 Meteorological parameters and satellite data of air masses, sea ice, and chlorophyll *a*

We measured various meteorological parameters, such as ambient temperature, relative humidity (RH), wind speed, and true wind direction, using an automated meteorological station located on the top deck of the R/V *Xuelong* (Fig. S1 and Table S2 in the Supplement).

To determine the type of air masses, we first conducted the 72 h back trajectory with daily resolution per each starting location using the NOAA Hybrid Single-Particle Lagrangian Integrated Trajectories (HYSPLIT, version 4.9) model (Fig. S2). Additionally, we conducted a 96 h back trajectory analysis with an hourly resolution, which covered the enhanced calcium enrichment events associated with sea ice fraction and chlorophyll *a* concentration (discussed in Sect. 3.1), using the TrajStat in Meteoinfo (version 3.5.8) (Wang et al., 2009; Wang, 2014). Meteorological data used for back trajectory analysis were obtained from the Global Data Assimilation System (GDAS; ftp://ftp.arl.noaa.gov/pub/archives, last access: 18 January 2023). Moreover, we obtained the monthly sea ice fraction from the Sea Ice Concentration Climate Data Record with a spatial resolution of 25 km (https://www.ncei.noaa.gov/products/climate-data-records/sea-ice-concentration, last access: 23 January 2023) and the 8 d chlorophyll *a* concentration from MODIS/Aqua with a spatial resolution of 4 km (https://modis.gsfc.nasa.gov, last access: 23 January 2023) (Fig. S3).

During the R/V *Xuelong* cruise observation campaigns, leg I was dominantly affected by the air masses from the sea-ice-covered open water (92 %, by trajectory coverage), and leg II was mainly affected by the air masses from continental Antarctica (58 %) (Table S2). The average ambient temperature (-4.1 ± 1.4 °C vs. -3.2 ± 2.2 °C), wind speed (7.2 ± 5.5 m s^{-1} vs. 7.1 ± 4.2 m s^{-1}), and chlorophyll *a* concentration (0.51 ± 0.29 µg L^{-1} vs. 0.44 ± 0.18 µg L^{-1}) varied slightly between legs I and II (Table S2).

2.3 Contamination control during observation campaigns

During the research cruise, the major contamination source was identified as emissions from a chimney located at the stern of the vessel and about 25 m above the sea surface. To mitigate the potential impact of ship emissions on aerosol sampling, we took several measures. Firstly, a total suspended particulate (TSP) sampling inlet connecting to the monitoring instruments was fixed to a mast 20 m above the sea surface, located at the bow of the vessel. In addition, the sampling inlet was fixed on a ship pillar with a rain cover, which could minimize the potential influence of violent shaking of the ship and sea waves. Secondly, sampling was only conducted while the ship was sailing, to avoid the possible effect of ship emission on aerosol sampling under low diffusion conditions. Lastly, we did not observe the mass spectral characteristics associated with ship emission (e.g., particles simultaneously contain m/z 51 $[V]^+$, 67 $[VO]^+$, and element carbon) during the observation campaigns (Liu et al., 2017; Passig et al., 2021). These measures ensured that the collected data were representative and reliable for subsequent analysis.

2.4 Instrumentation

An IGAC system (Model S-611, Machine Shop, Fortelice International Co. Ltd.) and a SPAMS instrument (Hexin Analytical Instrument Co., Ltd.) were synchronously employed to determine water-soluble ion mass concentrations of bulk aerosol and the size and chemical composition of individual particles in real time with hourly resolution (Figs. 2 and S4). In the aerosol sampling procedure, a TSP inlet with a PM_{10} cyclone (trap efficiency greater than 99 % for particles > 0.3 µm, $D_{a50} = 10 \pm 0.5$ µm) was used for IGAC sampling and a $PM_{2.5}$ cyclone ($D_{a50} = 2.5 \pm 0.2$ µm) to remove particles larger than 2.5 µm for SPAMS. All instruments were connected using conductive silicon tubing with an inner diameter of 1.0 cm.

2.4.1 Aerosol water-soluble ion constituents

The details of the analytical method of IGAC have been described in previous studies (Young et al., 2016; Yan et al., 2019, 2020b). Briefly, the IGAC system consisted of three main units, including a wet annular denuder (WAD), a scrub and impact aerosol collector (SIAC), and an ion chromatograph (IC; Dionex ICS-3000) (Fig. 2). Gases and aerosols were passed through the WAD with a sampling flow of 16.7 L min^{-1}. Two concentric Pyrex glass cylinders with a length of 50 cm and inner and outer diameters of 1.8 and 2.44 cm were fixed to the WAD, in which the inner walls of the annulus were wetted with ultrapure water (18.2 MΩ cm^{-1}). This part was responsible for the collection of acidic and basic gases by diffusion and absorption of a downward-flowing aqueous solution. The SIAC had a

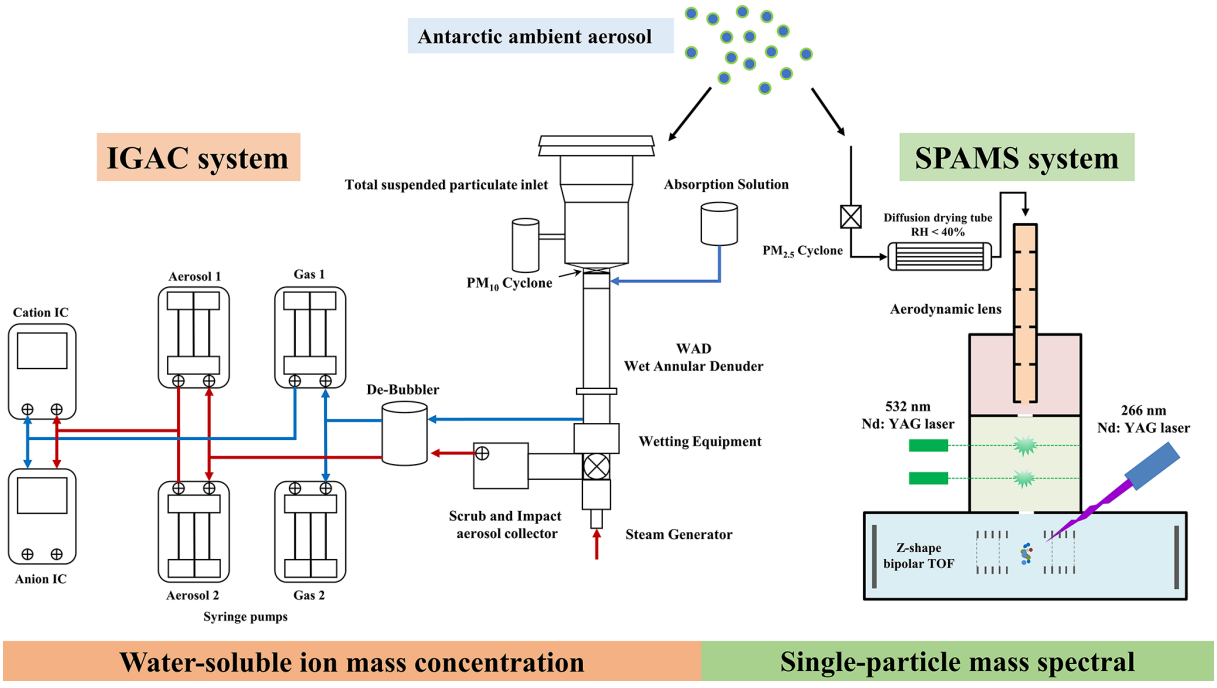

Figure 2. A schematic of the aerosol sampling system of IGAC and SPAMS during the research cruise over the Ross Sea, Antarctic.

length of 23 cm and a diameter of 4.75 cm, which was positioned at an angle to facilitate the collection of enlarged particles. The collected particles were separated firstly, continually enlarged by vapor steam, and then accelerated through a conical-shaped impaction nozzle and collected on an impaction plate. Each aerosol sample was collected for 55 min and injected for 5 min. The injection loop size was 500 µL for both anions and cations, which were subsequently analyzed by IC. The collection efficiency of aerosol and gas samples before they entered IC was previously reported higher than 89 % (for 0.056 µm particles, 89 %; for 1 µm particles, 98 %; for gas samples, > 90 %) (Chang et al., 2007; Tian et al., 2017). The target ion concentrations were calibrated with a coefficient of determination (r^2) above 0.99 using standard solutions (0.1–2000 µg L^{-1}). The detection limits for Na, Cl, Ca, K, and Mg were 0.03, 0.03, 0.019, 0.011, and 0.042 µg L^{-1} (aqueous solution), respectively. The systematic error of the IC systems was generally less than 5 %. The detection limits for Na^+, Cl^-, Ca^{2+}, K^+, and Mg^{2+} were 0.03, 0.03, 0.019, 0.011, and 0.042 µg L^{-1} (aqueous solution), respectively.

Throughout the observation campaigns, the mean Na^+ and Ca^{2+} mass concentrations were 364.64 ng m^{-3} (ranging from 6.66 to 4580.10 ng m^{-3}) and 21.20 ng m^{-3} (ranging from 0.27 to 334.40 ng m^{-3}), respectively, which were 10 times higher than the detection limits. Analytical uncertainty of Ca^{2+} enrichment based on water-soluble analysis was estimated at less than 11 % (Sect. S1 in the Supplement).

It should be clarified that the water-soluble ion mass concentration included the pure inorganic part (e.g., pure sea salt, NaCl) and mixed organic–inorganic part (e.g., gel-like particles) (Quinn et al., 2015). Numerous studies have reported that primary SSAs exhibited moderate hygroscopicity and water solubility due to a certain water-soluble organic fraction (∼ 25 %, by mass), such as carboxylates, lipopolysaccharides (LPSs), humic substances, and galactose (Oppo et al., 1999; Quinn et al., 2015; Schill et al., 2015; Cochran et al., 2017). For example, Oppo et al. (1999) indicated that humic substances were an important pool of water-soluble natural surfactants (40 %–60 %) in marine surfactant organic matter. In addition, LPSs are preferentially transferred to submicron SSAs during bubble bursting and exhibit a certain solubility of 5 g L^{-1} in pure water (Facchini et al., 2008; Schill et al., 2015). Therefore, both organic and inorganic parts with a water-soluble nature could be retained, contributing to the water-soluble ion mass concentration (e.g., Ca^{2+}).

2.4.2 Single-particle analysis

A brief description of SPAMS has been provided elsewhere (Li et al., 2011). Briefly, the aerosols were drawn into SPAMS by a $PM_{2.5}$ inlet after a silica gel dryer (Fig. 2). A collimated particle beam focused by an aerodynamic lens was then accelerated in an accelerating electric field and passed through two continuous laser beams (Nd:YAG laser, 532 nm). The obtained time of flight (TOF) and velocity of individual particles were used to calculate the vacuum aerodynamic diameter (D_{va}) based on a calibration curve. Subsequently, particles with a specific velocity were desorbed and ionized by triggering a pulse laser (an Nd:YAG laser,

266 nm, 0.6 ± 0.06 mJ was used in this study). The ion fragments were recorded using a bipolar TOF mass spectrometer. The detectable dynamic mass spectral ion signal is 5–20 000 mV. Before the use of SPAMS, standard polystyrene latex spheres (0.2–2 µm, Duke Scientific Corp.) and $PbCl_2$ and $NaNO_3$ (0.35 µm, Sigma-Aldrich) solutions were used for the size and mass spectral calibration, respectively. The hit rate, defined as the ratio of ionized particles to all sampled particles, of the SPAMS was ~ 11 % during the cruise observation campaigns.

During the R/V *Xuelong* cruise observation campaigns, approximately 930 000 particles with mass spectral fingerprints and D_{va} ranging from 0.2 to 2 µm were measured. An adaptive resonance theory neural network (ART-2a) was used to group the particles into several clusters based on their mass spectral fingerprints, using parameters of a vigilance factor of 0.85, a learning rate of 0.05, and a maximum of 20 iterations (Song and Hopke, 1999). The manually obtained clusters were sea salt (SS; 16.5 %), aged sea salt (SS-aged; 8.1 %), sea salt with biogenic organic matter (SS-Bio; 3.1 %), internally mixed organics with calcium (OC-Ca; 48.7 %), internally mixed organics with potassium (OC-K; 13.7 %), organic-carbon-dominated (OC; 7.0 %), and element carbon (EC; 2.9 %) (Fig. S5 and Table S3) (Prather et al., 2013; Collins et al., 2014; Su et al., 2021). All single-particle types had marine origins with typical mass spectral characteristics of Na (m/z 23), Mg (m/z 24), K (m/z 39), Ca (m/z 40), and Cl (m/z −35 and −37), except for EC (Sect. S2). There was little difference in individual particle analysis regarding chemical composition, size, and mixing state of particle clusters obtained from legs I and II (Sect. S3).

3 Results

3.1 Ca^{2+} enrichment dominated by environmental factors

We propose that both Na^+ and Ca^{2+} in our observations originated from marine sources. The mass concentration of Na^+ exhibited a strong positive correlation with that of Cl^- ($r = 0.99$, $p < 0.001$) and Mg^{2+} ($r = 0.99$, $p < 0.001$) (Fig. S6), indicating that they had a common origin (i.e., sea spray). However, it is not surprising that the mass concentration of Na^+ showed a relatively weak correlation with that of Ca^{2+} ($r = 0.51$, $p < 0.001$) (Fig. S6). This can be explained by the low water-soluble complexation of Ca^{2+} with organic matter and/or insoluble Ca^{2+} in the form of calcareous shell debris, such as $CaCO_3$. In addition, the potential impact of long-range transport of anthropogenic aerosols and dust contributing to Ca^{2+} may be limited due to the predominance of polar air masses during the observation campaigns (Fig. S2).

The enrichment factor (EF_x), defined as the mass concentration ratio of a specific species X to Na^+ in aerosols to that in bulk seawater, is generally used to describe the enrichment extent of species X in aerosols.

$$EF_x = \frac{([X]/[Na^+])_{aerosol}}{([X]/[Na^+])_{seawater}}$$

An $EF_x > 1$ indicates a positive enrichment; otherwise, it indicates depletion. Generally, the ratio of Ca^{2+} to Na^+ in seawater is 0.038 (w/w) (Boreddy and Kawamura, 2015; Su et al., 2022). During the whole cruise, the hourly average EF_{Ca} was 2.76 ± 6.27 (mean ± standard deviation (M ± SD), $n = 1051$, ranged from 0.01 to 85, median = 1.18, interquartile range (IQR) = 1.85). Similar to previous studies (Salter et al., 2016), positive magnesium (Mg^{2+}) and potassium (K^+) enrichment in SSAs was also observed (Sect. S4).

Figure 3 presents the enrichment factor of Ca^{2+} (EF_{Ca}) at different ambient temperatures (separated by a mean value of −3.5 °C) and wind speeds (separated by a mean value of 7 m s^{-1}) and in the presence/absence of sea ice during the entire observation campaign. The results indicated that the highest EF_{Ca} zone ($M \pm SD = 3.83 \pm 3.43$, median = 2.66, IQR = 3.37, $n = 144$) occurred at a lower ambient temperature (< −3.5 °C) and lower wind speed (< 7 m s^{-1}) and in the presence of sea ice (Fig. 3d). Compared to the contrary conditions (i.e., ambient temperatures ≥ −3.5 °C, wind speeds ≥ 7 m s^{-1}, and the absence of sea ice), there was almost calcium depletion (EF_{Ca}, $M \pm SD = 1.01 \pm 0.80$, median = 0.70, IQR = 0.73, $n = 182$) (Fig. 3c). Notably, we observed a higher EF_{Ca} during the sea ice period than during the period without sea ice (3.83 ± 3.43 vs. 2.45 ± 3.09 by M ± SD and 2.66 vs. 1.18, by median) (Fig. 3d), under the conditions of ambient temperatures < −3.5 °C and wind speeds < 7 m s^{-1}. In addition, we also observed more frequent Ca^{2+} enrichment events during the sea ice period (71.0 % in leg I) compared to the period without sea ice (47.7 % in leg II) (Table S2). Moreover, the increased EF_{Ca} varied with decreasing ambient temperature and wind speed and with increasing sea ice fraction, as shown in Fig. 4. Taken together, our results indicate that the enhanced Ca^{2+} enrichment in SSAs is sensitive to the lower temperature, lower wind speeds, and the presence of sea ice.

We further analyzed the distribution of Ca^{2+} enrichment concerning 96 h back trajectories with sea ice fraction and chlorophyll a concentration, as shown in Fig. 5. During the observation campaigns, we identified five areas with continuous enhancement of Ca^{2+} enrichment, namely, Areas 1 and 2 during leg II and Areas 3, 4, and 5 during leg I. Our results indicated that air masses traveling over the sea ice and marginal ice zone (> 95 %, by trajectory coverage) in Areas 3, 4, and 5, as well as those over the sea-ice-based (28 %–33 %) and land-based Antarctic ice (57 %–59 %) in Areas 1 and 2, were strongly associated with the increased calcium enrichment (Table S4). These pieces of evidence further support the influence of sea ice on the increased calcium enrichment, while simultaneously ruling out the influence of long-range transport of anthropogenic aerosol and dust outside the Antarctic.

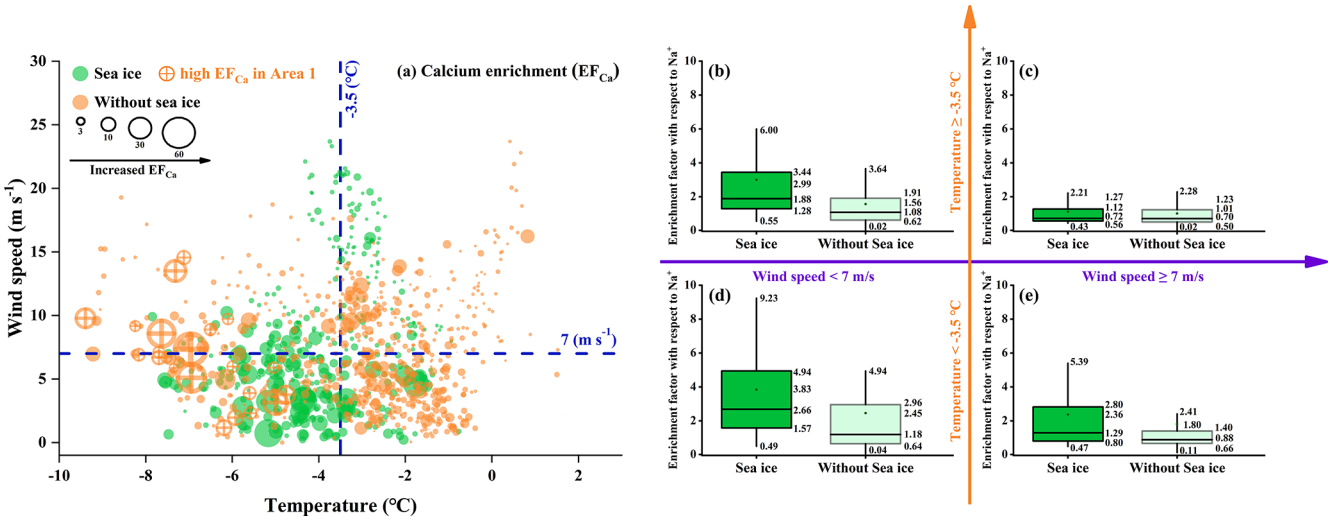

Figure 3. **(a)** Bubble chart of the hourly Ca^{2+} enrichment factor (EF_{Ca}) with respect to Na^{+} with different environmental factors (ambient temperature, wind speed, and sea ice fraction). The green and orange dots represent the EF_{Ca} values for the periods with and without sea ice, respectively. The marked orange dots represent a series of high EF_{Ca} cases that were correlated with a high concentration of chlorophyll *a* during leg II of the cruise. **(b–e)** Data support of the bubble chart represented by box-and-whisker plots. In the box-and-whisker plots, the marked values from top to bottom are the 90th and 75th percentiles, mean, median, and 25th and 10th percentiles, respectively.

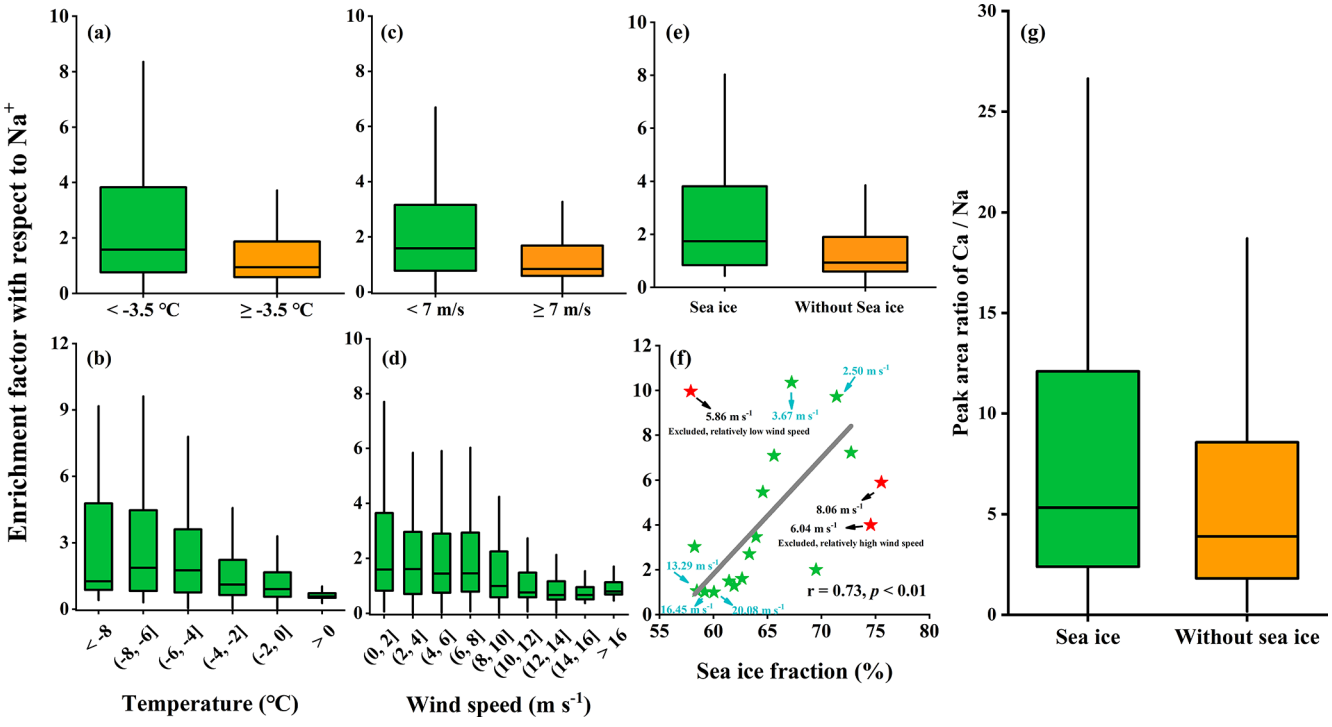

Figure 4. Enrichment factors of Ca^{2+} with respect to Na^{+} varied as a function of the ambient temperature **(a–b)**, wind speed **(c–d)**, and sea ice fraction **(e–f)** during cruise observation campaigns. **(g)** A box-and-whisker plot of the single-particle peak area ratio of Ca/Na in OC-Ca for the periods with and without sea ice. In the box-and-whisker plots, the lower, median, and upper lines of the box denote the 25th, 50th, and 75th percentiles, respectively. The lower and upper edges denote the 10th and 90th percentiles, respectively. The solid black star **(f)** exhibited an anomalous trend due to its nature of relatively high or low wind speed. The first point exhibited a high EF value because of its relatively low wind speed (5.86 m s^{-1}). The second and third points exhibited low EF values because of their relatively high wind speeds of 6.04 and 8.06 m s^{-1}, respectively. These three points have been excluded from the correlation analysis.

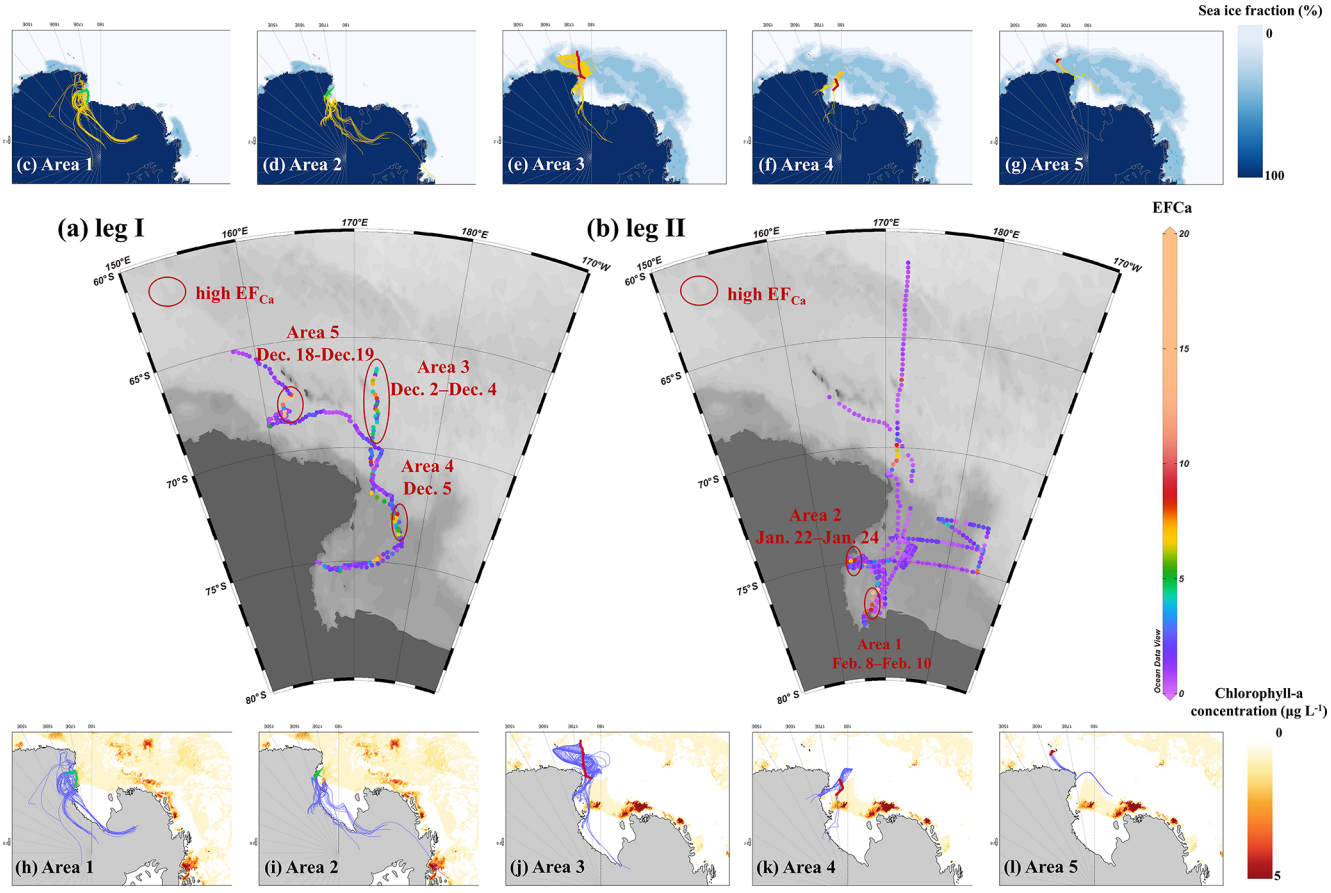

Figure 5. Distribution of EF_{Ca} during **(a)** leg I and **(b)** leg II. Five distinct areas with continuous enhanced Ca^{2+} enrichment events, along with 96 h back trajectories (one trajectory per hour in each starting condition), sea ice fraction (**c**–**g**, yellow traces), and chlorophyll *a* concentration (**h**–**l**, light-blue traces). Lines in red and green referred to ship tracks for corresponding areas during legs I and II, respectively.

We observed that a series of high EF_{Ca} cases in Area 1 were associated with a high concentration of chlorophyll *a* ($0.99 \pm 1.65\,\mu g\,L^{-1}$). However, it is unlikely that phytoplankton and/or bacteria are responsible for the enhanced EF_{Ca} cases due to the weak correlation ($r = 0.12$, $p < 0.01$) between the chlorophyll *a* concentration and EF_{Ca} values (Fig. S7). Moreover, although the ship track of leg II covered large areas with high chlorophyll *a* concentrations, the high EF_{Ca} values were only present at the narrow temporal and spatial scales. Furthermore, results from back trajectories indicated that air masses did not significantly travel through the region with elevated chlorophyll *a* concentration. Therefore, we suggest that the impact of chlorophyll *a* concentration on Ca^{2+} enrichment may be limited.

3.2 Single-particle characteristics of Ca-containing particles

To elucidate the mixing state of individual calcareous particles, we set a threshold for the ion count rate of m/z 40 $[Ca]^+$ (ion intensity > 100 mV) to reclassify all single-particle types that were obtained from the ART-2a algorithm. This means that all reclassified particles contain signals of m/z 40 $[Ca]^+$. A total of ~ 580 000 Ca-containing particles were distributed among all particle types, accounting for ~ 62 % of the total obtained particles. OC-Ca was the dominant (~ 72 %, by occurrence frequency) particle type among all Ca-containing particles, followed by SS-Ca (calcium-containing sea salt; ~ 12 %) (Fig. 6h). Each of the remaining particle types accounted for negligible fractions (< 7 %) in the total of Ca-containing particles and were classified as "other". Thus, they were not included in the following discussion.

OC-Ca was characterized by a prominent ion signature for m/z at 40 $[Ca]^+$ in the positive mass spectrum and organic marker ions of biological origin (e.g., organic nitrogen, phosphate, carbohydrate, siliceous materials, and organic carbon) in the negative spectrum (Fig. 6d). Specifically, organic nitrogen (m/z −26 $[CN]^-$ and −42 $[CNO]^-$) showed the largest number fraction (NF) at ~ 88 % (Fig. S5h), which is likely derived from organic nitrogen species, such as amines, amino groups, and/or cellulose (Czerwieniec et al., 2005; Srivastava et al., 2005; Köllner et al., 2017; Dall'Osto et

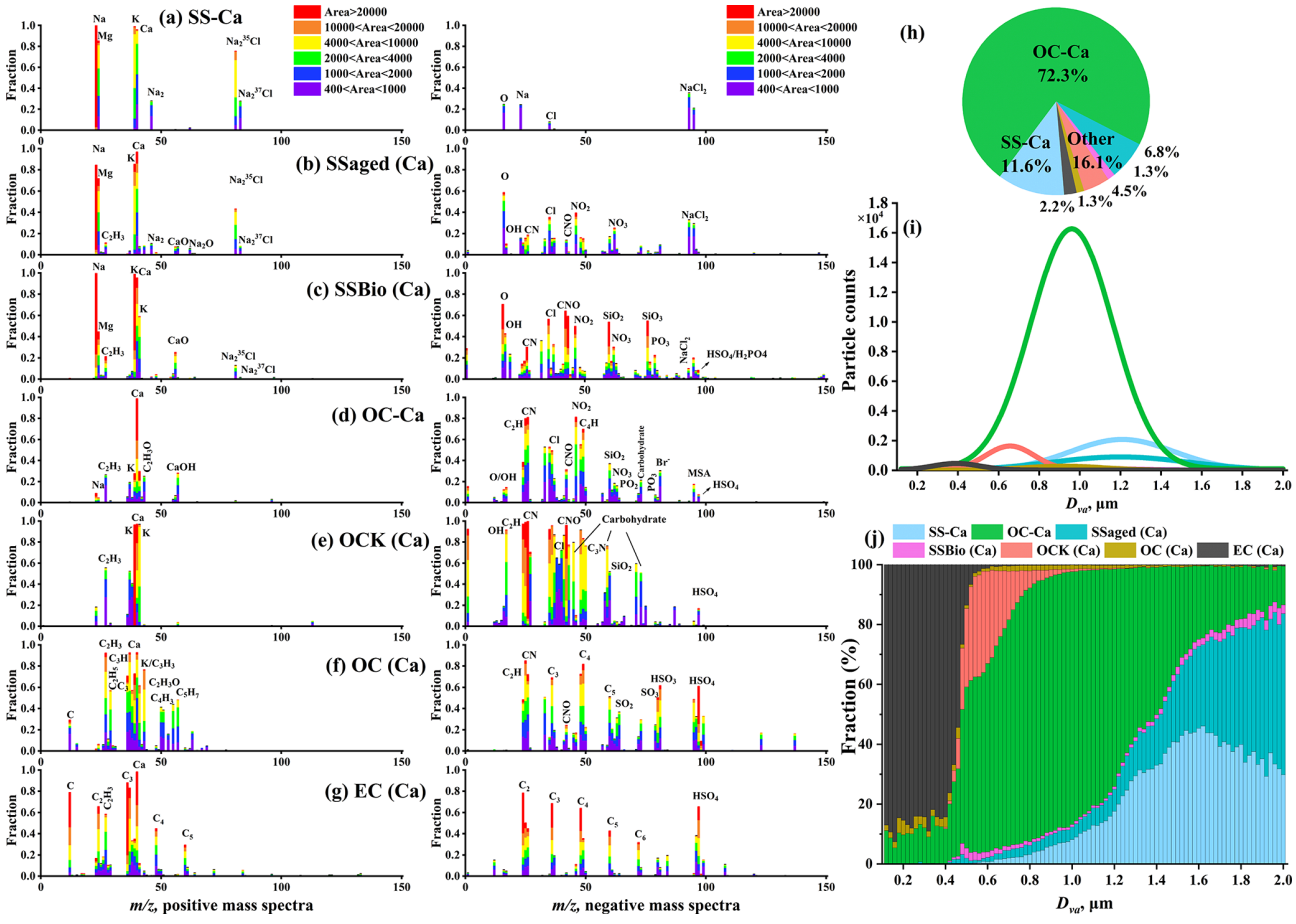

Figure 6. **(a–g)** Average digitized single-particle mass spectra of seven chemical classes of Ca-containing particles. New single-particle types are reclassified with m/z 40 $[Ca]^+$ based on previous ART-2a results. **(h)** Relative proportion and **(i)** unscaled size-resolved number distributions of single-particle types using Gaussian fitting. **(j)** Number fractions of single-particle types per size bin versus particle size.

al., 2019). Higher NFs of phosphate (16 %; m/z −63 $[PO_2]^-$ and −79 $[PO_3]^-$), carbohydrates (24 %; m/z −45 $[CHO_2]^-$, −59 $[C_2H_3O_2]^-$, and −73 $[C_3H_5O_2]^-$), siliceous materials (40 %;m/z −60 $[SiO_2]^-$), and organic carbon (37 %; m/z 27 $[C_2H_3]^+$ and m/z 43 $[C_2H_3O]^+$) were also observed in OC-Ca relative to other particle types (Fig. S5h). These organic ion signatures likely correspond to phospholipids, mono- and polysaccharides, and biosilica structures (e.g., exoskeletons or frustules), which may be derived from the intact heterotrophic cells, fragments of cells, and exudates of phytoplankton and/or bacteria (Prather et al., 2013; Guasco et al., 2014; Zhang et al., 2018). In addition, the strong organic ion intensities may truly reflect the amount of organic material in OC-Ca because the particles are sufficiently dry during the ionization process (i.e., complete positive and negative mass spectra) (Gross et al., 2000). Notably, the possible ion signals of bromide (m/z −79 and −81) were observed in OC-Ca, indicating a potential source of blowing snow (Yang et al., 2008; Song et al., 2022).

The OC-Ca particles are most likely classified as a distinct SSA population, probably of marine biogenic origin. Sea salt particles typically exhibit a stronger m/z 23 $[Na]^+$ than m/z 40 $[Ca]^+$ due to the higher concentration of Na^+ vs. Ca^{2+} in seawater and also due to the lower ionization potential of Na vs. Ca (5.14 eV vs. 6.11 eV) (Gross et al., 2000). However, the ratio of m/z 23 $[Na]^+$ to m/z 40 $[Ca]^+$ in the OC-Ca particles is reversed, verifying a distinct single particle type (Gross et al., 2000; Gaston et al., 2011). Similarly, the ion signal of m/z 39 $[K]^+$ does not surpass that of m/z 40 $[Ca]^+$ in OC-Ca, although K is ionized more easily than Ca (4.34 eV vs. 6.11 eV) (Gross et al., 2000). Although RH at the sampling outlet was < 40 %, the short residence time of the particles within the drying tube (< 5 s) and vacuum system (< 1 ms) could have been insufficient for the complete efflorescence of SSAs (Gaston et al., 2011; Sierau et al., 2014). Hence, the OC-Ca could not be attributed to the chemical fractionation of the efflorescence SSAs in SPAMS analysis. Additionally, based on the single-particle mass spectrometry technique, some particle types with similar chemical char-

acteristics to OC-Ca have been observed in both field and laboratory studies (e.g., atomization of sea ice meltwater collected in the Southern Ocean) (Gaston et al., 2011; Prather et al., 2013; Collins et al., 2014; Guasco et al., 2014; Dall'Osto et al., 2019; Su et al., 2021). The OC-Ca may be from local emissions because the measurements were almost entirely influenced by polar air masses (Fig. S2). Other possible sources, such as glacial dust (Tobo et al., 2019), could be excluded because of the lack of crustal mass spectral characteristics (e.g., -76 $[SiO_3]^-$, 27 $[Al]^+$, and 48 $[Ti]^+/64$ $[TiO]^+$) (Pratt et al., 2009; Zawadowicz et al., 2017). And the mean mass concentration ratio of Ca/Na in the aerosol sample was only 0.10, much lower than that in the crust (1.78, w/w).

In contrast, SS-Ca was classified as a pure inorganic cluster with predominant contributions of Na-related compounds (m/z 23 $[Na]^+$, 46 $[Na_2]^+$, 81/83 $[Na_2^{35/37}Cl]^+$, and $-93/-95$ $[Na^{35/37}Cl_2]^-$), Mg (m/z 24), K (m/z 39), and Ca (m/z 40) in the mass spectra (Fig. 6a). Organic ion signals such as organic nitrogen (m/z -26 $[CN]^-$ and -42 $[CNO]^-$) and phosphate (m/z -63 $[PO_2]^-$ and -79 $[PO_3]^-$) were rarely detected ($\sim 1\,\%$, by NF). As described above, these compounds relate to oceanic biogeochemical processes. In addition, secondary species (e.g., nitrate of m/z -62 $[NO_3]^-$ and sulfate of m/z -97 $[HSO_4]^-$) were also not observed, indicating a fresh origin and/or less atmospheric aging. As a subpopulation of SS, SS-Ca may originate from bubble bursting within open water and/or blowing snow.

4 Discussion

SS-Ca (calcium-containing sea salt) represents a mixture of NaCl and $CaCl_2$. However, the SS-Ca showed a weak correlation ($r = 0.21$, $p < 0.05$, by count and $r = 0.03$, $p < 0.05$, by the peak area of m/z 40 $[Ca]^+$) with the mass concentration of Ca^{2+} (Table 1). In addition, the proportion of SS-Ca was also small (11.6 %, Fig. 6h). These results indicate that $CaCl_2$ is not the major reason for the Ca^{2+} enrichment in SSAs, although $CaCl_2$ has been proposed as a cause, based on laboratory atomizing of pure inorganic artificial seawater (Salter et al., 2016). The contribution of ikaite ($CaCO_3 \cdot 6H_2O$) could also be excluded due to its low water solubility (Bischoff et al., 1993; Dieckmann et al., 2008, 2010), although ikaite from sea salt fractionation has also been proposed to account for the Ca^{2+} enrichment in SSAs over the Antarctic coast (Hara et al., 2012). Moreover, the mass spectral signatures of $CaCO_3$ (e.g., m/z 56 $[CaO]^+$ and -60 $[CO_3]^-$ (see Sullivan et al., 2009) were also rare in the SS-Ca particles (Fig. 6a).

As a major component ($\sim 72\,\%$, by occurrence frequency) of the Ca-containing particles, OC-Ca is expected to be partially responsible for the calcium enrichment in SSAs. First, the OC-Ca and mass concentration of Ca^{2+} exhibited moderately weak positive correlations ($r = 0.42$, $p < 0.05$, by count and $r = 0.49$, $p < 0.05$, by the peak area of m/z 40 $[Ca]^+$) and moderately strong correlations under higher EF_{Ca} values ($EF_{Ca} > 10$, $r = 0.63$, $p < 0.05$, by count and $r = 0.68$, $p < 0.05$, by the peak area of m/z 40 $[Ca]^+$) (Table 1). Also, such correlations were great during leg I ($r = 0.59$, $p < 0.05$, by count and $r = 0.60$, $p < 0.05$, by the peak area of m/z 40 $[Ca]^+$). Second, the OC-Ca showed a size distribution with a peak at 1 µm (Fig. 6i), which is consistent with the significant Ca^{2+} enrichment that is generally found in submicron SSAs (Cochran et al., 2016; Salter et al., 2016; Mukherjee et al., 2020).

We further show that calcium may strongly mix with organic matter, probably as organically complexed calcium, in the OC-Ca particles. The calcium correlated well with different kinds of organic matter (e.g., phosphate, $r = 0.81$, $p < 0.05$, by the peak area) but correlated poorly with chloride ($r = 0.21$, $p < 0.05$, by the peak area and $r = 0.48$, $p < 0.05$, by mass concentration) (Fig. S6). In addition, different kinds of organic matter (e.g., organic nitrogen, organic carbon) in the OC-Ca particles also showed enrichment trends below the submicron level, analogously to Ca^{2+} enrichment (Fig. S8). Particularly, EF_{Ca} and organic nitrogen (with the largest NF in OC-Ca) were both affected by the environmental factors of ambient temperature, wind speed, and sea ice fraction, indicating possible organic binding with calcium (Fig. S9).

To exclude the potential inorganic water-soluble compounds (i.e., chloride (m/z -35 and -37), nitrate (m/z -62), and sulfate (m/z -97)), we further classified OC-Ca into two subpopulations, OC-Ca-Organic (23.6 %, by proportion) and OC-Ca-Inorganic (48.7 %, by proportion) (Fig. S10), depending on the presence of inorganic ion signals (i.e., chloride of m/z $-35/-37$ $[Cl]^-$, nitrate of m/z -62 $[NO_3]^-$, and sulfate of m/z -97 $[HSO_4]^-$). Both the OC-Ca types and mass concentrations of Ca^{2+} showed enhanced correlations under high EF_{Ca} values (Table 1). In particular, OC-Ca-Organic exhibited stronger correlations than OC-Ca-Inorganic did ($r = 0.51$ vs. $r = 0.28$, $p < 0.05$, by count and $r = 0.51$ vs. 0.31, $p < 0.05$, by the peak area of m/z 40 $[Ca]^+$, respectively), which indicates the importance of OC-Ca-Organic for the enrichment of Ca^{2+}. Although we did not measure the hygroscopicity of the OC-Ca in this study, we infer it to be hygroscopic to some extent. As reported by Cochran et al. (2017), the mixture of sea salt with organic matter can also exhibit a certain hygroscopicity (hygroscopicity parameter, 0.50–1.27). Therefore, it is likely that the organically complexed calcium is slightly water-soluble and is partially responsible for calcium enrichment, while current studies may neglect it.

The possible processes contributing to the calcium enrichment induced by OC-Ca can only be speculated on (Fig. 7). Ca^{2+} tends to bind with organic matter of biogenic origin, such as exopolymer substances (EPSs), and subsequently assemble as marine microgels (Verdugo et al., 2004; Gaston et al., 2011; Krembs et al., 2011; Orellana et al., 2011; Verdugo, 2012; Orellana et al., 2021). Large amounts of mi-

Table 1. Correlation analysis between the OC-Ca (by count and by the peak area of m/z 40 $[Ca]^+$) and its two subpopulations OC-Ca-Organic and OC-Ca-Inorganic, SS-Ca (by count and by the peak area of m/z 40 $[Ca]^+$), and mass concentration of Ca^{2+} in the variation of EF_{Ca}, with the p value < 0.05.

EF_{Ca}	Count (Correlation coefficient, r)				Peak area (Correlation coefficient, r, m/z 40 $[Ca]^+$)			
	OC-Ca-Inorganic	OC-Ca-Organic	OC-Ca	SS-Ca	OC-Ca-Inorganic	OC-Ca-Organic	OC-Ca	SS-Ca
0–5	0.08	0.31	0.18	0.07	0.18	0.44	0.41	0.04
5–10	0.15	0.37	0.27	0.04	0.14	0.36	0.33	0.06
> 10	0.58	0.59	0.63	0.10*	0.53	0.68	0.68	0.10
Leg I	0.45	0.59	0.55	0.02	0.53	0.60	0.60	0.03
Leg II	0.06	0.22	0.14	0.45	0.14	0.39	0.39	0.11
Total	0.28	0.51	0.42	0.21	0.31	0.51	0.49	0.03

* p value > 0.05 (Pearson method, two-tailed test).

crogels, driven by sea ice algae, microorganisms, and/or exchanges of organic matter with the seawater below, stick to the sea ice due to its porous nature. Furthermore, they are likely to be present in the snow, frost flowers, and brine channels (Krembs et al., 2002; Gao et al., 2012; Vancoppenolle et al., 2013; Arrigo, 2014; Boetius et al., 2015; Kirpes et al., 2019). A low wind speed may not only be conducive to the formation of frost flowers and snow but also produce less sea salt (i.e., small yields of Na^+ relative to Ca^{2+}) (Rankin et al., 2002). Correspondingly, a high wind speed ($\geq 7\,m\,s^{-1}$) can yield more sea salt by blowing-snow events and/or wave breaking (Yang et al., 2008; Song et al., 2022), presenting a dilution effect of Na^+ on Ca^{2+}. In this case, the calcium enrichment in SSAs could reasonably be attributed to the possible gel-like calcium-containing particles released by low-wind-blown sea ice. This inference is supported by the observation of air masses blown over a large fraction of sea-ice- or land-based Antarctic ice, as well as a moderate negative correlation ($r = -0.50$, $p < 0.001$) between wind speed and sea ice fraction. In addition, we also observed a higher proportion of OC-Ca at low wind speeds ($< 7\,m\,s^{-1}$, 61.5 %) than at high wind speeds ($\geq 7\,m\,s^{-1}$, 38.5 %). Coincidently, Song et al. (2022) also reported that a low-wind-blown sea ice process can drive the biogenic aerosol response in the high Arctic. In addition, the enhanced presence of film drops was observed at lower wind speeds ($< 6\,m\,s^{-1}$) (Norris et al., 2011), which suggests that the bubble bursts within the sea ice leads and open water may also be responsible for the release of OC-Ca and its calcium enrichment involved (Leck and Bigg, 2005a, b; Bigg and Leck, 2008; Leck and Bigg, 2010; Leck et al., 2013; Kirpes et al., 2019).

As expected, the results of the Ca^{2+} enrichment in SSAs obtained from ion mass concentration via IGAC did not fully align with results from SPAMS datasets. We propose two possible explanations for this discrepancy: (i) it could be attributed to a difference in the size of particles collected by the two different instruments ($\sim 10\,\mu m$ for IGAC and 0.2–2 µm for SPAMS). In addition, SPAMS cannot measure the Aitken-mode particles (Sierau et al., 2014) and can measure only the tail of accumulation-mode particles with a relatively low hit rate ($\sim 11\,\%$ in this study). (ii) The types of datasets obtained via IGAC (ion mass concentration) and SPAMS (mass spectral characteristics) are different. The former method partially reflects the Ca^{2+} distribution based on water-soluble Ca^{2+}, while the OC-Ca measured by SPAMS may have low water solubility. The latter method is still challenging to use for quantitative measurements due to potential inhomogeneities in the transmission efficiencies of the aerodynamic lenses and desorption/ionization, as well as the matrix effects of individual particles (Gross et al., 2000; Qin et al., 2006; Pratt and Prather, 2012). Therefore, it may not be straightforward to compare the particle count and peak area with the absolute mass concentration.

Although there is a discrepancy between the two instruments, we believe our results to be reliable and representative. On the one side, the quantitative results concluded by IGAC confirm the enrichment of Ca^{2+} in SSAs and demonstrate their dependence on and relevance to the environmental factors. On the other side, the individual particle analysis ranging in size from 0.2 to 2 µm is highly appropriate for revealing the calcium distribution in SSAs, as previous studies have shown increasing Ca^{2+} enrichment in SSAs below 1 µm (Oppo et al., 1999; Hara et al., 2012; Cochran et al., 2016; Salter et al., 2016; Mukherjee et al., 2020). Our study successfully identifies a unique calcareous particle type (i.e., OC-Ca) and its specific mixing state. A comprehensive understanding of the characteristics of OC-Ca to the mechanisms of calcium enrichment is essential for further recognizing the CCN and IN activation in remote marine areas.

Another limitation is that only several environmental factors were considered for calcium enrichment in this study. Some potential factors, such as surface net solar radiation, snowfall, total cloud cover, surface pressure, total precipitation, boundary layer height, and seawater salinity, may also affect the calcium enrichment in SSAs through regulating the yield of sea salt (i.e., Na^+ mass concentration) (Song et

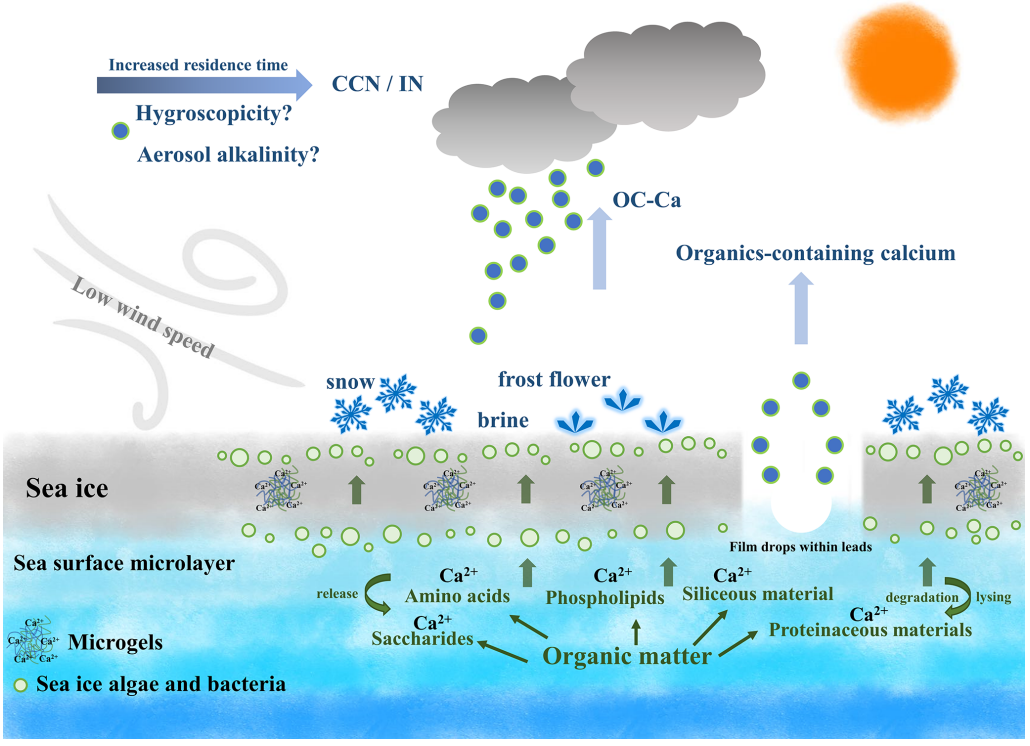

Figure 7. Schematic of the production of OC-Ca and its possible atmospheric implications beyond calcium enrichment. Ca^{2+} tends to bind with organic matter within sea ice/seawater and subsequently assemble as marine microgels, likely present in the snow, frost flowers, and brine channels. With the low-wind-blown sea ice process and/or bubble bursting within sea ice leads, these gel-like particles (i.e., OC-Ca) may be released to the Antarctic atmosphere, as a potential source of CCN/IN. Notably, the dataset via SPAMS cannot directly identify marine microgels. OC-Ca was likely associated with marine microgels, as calcium and biological organic material were extensively internally mixed. This OC-Ca type has previously been observed in the laboratory simulation of Collins et al. (2014).

al., 2022). However, they were not available in this study because of the lack of measurement during the cruise. Meanwhile, the satellite data with low temporal-spatial resolution cannot match per hour in each starting condition. We hope that future research will further investigate the enrichment of specific species in SSAs under a wider range of meteorological or oceanographic conditions.

5 Conclusions and atmospheric implications

We investigated the distribution of calcium in SSAs through the R/V *Xuelong* cruise observation campaigns over the Ross Sea, Antarctica. The most significant Ca^{2+} enrichment in SSAs occurred under relatively lower ambient temperatures ($< -3.5\,°C$) and wind speeds ($< 7\,m\,s^{-1}$) and with the presence of sea ice. With the help of individual particle mass spectral analysis, we first propose that a single-particle type of OC-Ca (internally mixed organics with calcium), probably resulting from the preferential binding of Ca^{2+} with organic matter, could partially account for the calcium enrichment in SSAs. We speculate that OC-Ca is likely produced from the effects of low-wind-blown sea ice on microgels induced by Ca^{2+} and/or the bubble bursts in the open water and/or sea ice leads. However, the impact of environmental factors and OC-Ca on calcium enrichment in SSAs still cannot be well predicted by multiple linear regression and random forest analysis (Sect. S5), which may be ascribed to other unknown mechanisms and/or organically complexed calcium with low water solubility. In addition, our conclusions based on limited spatial, temporal, meteorological, and oceanographic conditions may not be accessible to other seasons and oceanic basins.

We suggest that the environmental behaviors of the possible gel-like calcium-containing particles (i.e., OC-Ca) should be paid more attention behind the mechanisms of calcium enrichment. Under the stimulation of specific environmental factors (e.g., pH, temperature, chemical compounds, pollutants, and UV radiation), their physicochemical properties would be changed (e.g., water-solubility enhanced by the cleavage of polymers) (Orellana and Verdugo, 2003; Orellana et al., 2011). Such particles may be preferred candidates for CCN and/or IN (Willis et al., 2018; Lawler et al., 2021). To our knowledge, this is the first report of a calcium-dominated single-particle type OC-Ca in the Antarctic. In the context of global warming and sea ice retreat, this work provides insight into the chemical composition and distri-

bution of submicron SSAs in the Antarctic summer atmosphere, which would be helpful for a better understanding of aerosol–cloud–climate interactions.

Data availability. The data are available at Zenodo (https://doi.org/10.5281/zenodo.8279334; Su et al., 2023). Details can be accessed by contacting the corresponding author Guohua Zhang (zhanggh@gig.ac.cn) and the first author Bojiang Su (subojiang21@mails.ucas.ac.cn).

Supplement. The supplement related to this article is available online at: https://doi.org/10.5194/acp-23-10697-2023-supplement.

Author contributions. The idea for the study was conceived by BS. BS analyzed the data, prepared the figures, and wrote the manuscript under the guidance of GZ and XB. LL and JY contributed to the observation data. All co-authors contributed to the discussions of the results and refinement of the manuscript.

Competing interests. The contact author has declared that none of the authors has any competing interests.

Disclaimer. Publisher's note: Copernicus Publications remains neutral with regard to jurisdictional claims in published maps and institutional affiliations.

Acknowledgements. We appreciate the Chinese Arctic and Antarctic Administration for its support in fieldwork. The authors would like to thank the editor and reviewers for their valuable time and feedback.

Financial support. This work was supported by the National Natural Science Foundation of China (grant nos. 42222705 and 42377097), the Youth Innovation Promotion Association CAS (grant no. 2021354), the Guangdong Basic and Applied Basic Research Foundation (grant no. 2019B151502022), and the Guangdong Foundation for Program of Science and Technology Research (grant no. 2020B1212060053).

Review statement. This paper was edited by Tuukka Petäjä and reviewed by two anonymous referees.

References

Arrigo, K. R.: Sea ice ecosystems, Annu. Rev. Mar. Sci., 6, 439–467, https://doi.org/10.1146/annurev-marine-010213-135103, 2014.

Bertram, T. H., Cochran, R. E., Grassian, V. H., and Stone, E. A.: Sea spray aerosol chemical composition: elemental and molecular mimics for laboratory studies of heterogeneous and multiphase reactions, Chem. Soc. Rev., 47, 2374–2400, https://doi.org/10.1039/c7cs00008a, 2018.

Bigg, E. K. and Leck, C.: The composition of fragments of bubbles bursting at the ocean surface, J. Geophys. Res.-Atmos., 113, D11209, https://doi.org/10.1029/2007jd009078, 2008.

Bischoff, J. L., Fitzpatrick, J. A., and Rosenbauer, R. J.: The Solubility and Stabilization of Ikaite ($CaCO_3 \cdot 6H_2O$) from 0° to 25 °C: Environmental and Paleoclimatic Implications for Thinolite Tufa, The Journal of Geology, 101, 21–33, https://doi.org/10.1086/648194, 1993.

Boetius, A., Anesio, A. M., Deming, J. W., Mikucki, J. A., and Rapp, J. Z.: Microbial ecology of the cryosphere: sea ice and glacial habitats, Nat. Rev. Microbiol., 13, 677–690, https://doi.org/10.1038/nrmicro3522, 2015.

Boreddy, S. K. R. and Kawamura, K.: A 12-year observation of water-soluble ions in TSP aerosols collected at a remote marine location in the western North Pacific: an outflow region of Asian dust, Atmos. Chem. Phys., 15, 6437–6453, https://doi.org/10.5194/acp-15-6437-2015, 2015.

Brooks, S. D. and Thornton, D. C. O.: Marine Aerosols and Clouds, Annu. Rev. Mar. Sci., 10, 289–313, https://doi.org/10.1146/annurev-marine-121916-063148, 2018.

Carter-Fenk, K. A., Dommer, A. C., Fiamingo, M. E., Kim, J., Amaro, R. E., and Allen, H. C.: Calcium bridging drives polysaccharide co-adsorption to a proxy sea surface microlayer, Phys. Chem. Chem. Phys., 23, 16401–16416, https://doi.org/10.1039/d1cp01407b, 2021.

Chi, J. W., Li, W. J., Zhang, D. Z., Zhang, J. C., Lin, Y. T., Shen, X. J., Sun, J. Y., Chen, J. M., Zhang, X. Y., Zhang, Y. M., and Wang, W. X.: Sea salt aerosols as a reactive surface for inorganic and organic acidic gases in the Arctic troposphere, Atmos. Chem. Phys., 15, 11341–11353, https://doi.org/10.5194/acp-15-11341-2015, 2015.

Cochran, R. E., Jayarathne, T., Stone, E. A., and Grassian, V. H.: Selectivity Across the Interface: A Test of Surface Activity in the Composition of Organic-Enriched Aerosols from Bubble Bursting, J. Phys. Chem. Lett., 7, 1692–1696, https://doi.org/10.1021/acs.jpclett.6b00489, 2016.

Cochran, R. E., Laskina, O., Trueblood, J. V., Estillore, A. D., Morris, H. S., Jayarathne, T., Sultana, C. M., Lee, C., Lin, P., Laskin, J., Laskin, A., Dowling, J. A., Qin, Z., Cappa, C. D., Bertram, T. H., Tivanski, A. V., Stone, E. A., Prather, K. A., and Grassian, V. H.: Molecular Diversity of Sea Spray Aerosol Particles: Impact of Ocean Biology on Particle Composition and Hygroscopicity, Chem, 2, 655–667, https://doi.org/10.1016/j.chempr.2017.03.007, 2017.

Collins, D. B., Zhao, D. F., Ruppel, M. J., Laskina, O., Grandquist, J. R., Modini, R. L., Stokes, M. D., Russell, L. M., Bertram, T. H., Grassian, V. H., Deane, G. B., and Prather, K. A.: Direct aerosol chemical composition measurements to evaluate the physicochemical differences between controlled sea spray aerosol generation schemes, Atmos. Meas. Tech., 7, 3667–3683, https://doi.org/10.5194/amt-7-3667-2014, 2014.

Cravigan, L. T., Mallet, M. D., Vaattovaara, P., Harvey, M. J., Law, C. S., Modini, R. L., Russell, L. M., Stelcer, E., Cohen, D. D., Olsen, G., Safi, K., Burrell, T. J., and Ristovski, Z.: Sea spray aerosol organic enrichment, water uptake and

surface tension effects, Atmos. Chem. Phys., 20, 7955–7977, https://doi.org/10.5194/acp-20-7955-2020, 2020.

Czerwieniec, G. A., Russell, S. C., Tobias, H. J., Pitesky, M. E., Fergenson, D. P., Steele, P., Srivastava, A., Horn, J. M., Frank, M., Gard, E. E., and Lebrilla, C. B.: Stable isotope labeling of entire *Bacillus atrophaeus* spores and vegetative cells using bioaerosol mass spectrometry, Anal. Chem., 77, 1081–1087, https://doi.org/10.1021/ac0488098, 2005.

Dall'Osto, M., Airs, R. L., Beale, R., Cree, C., Fitzsimons, M. F., Beddows, D., Harrison, R. M., Ceburnis, D., O'Dowd, C., Rinaldi, M., Paglione, M., Nenes, A., Decesari, S., and Simo, R.: Simultaneous Detection of Alkylamines in the Surface Ocean and Atmosphere of the Antarctic Sympagic Environment, ACS Earth Space Chem., 3, 854–862, https://doi.org/10.1021/acsearthspacechem.9b00028, 2019.

Dieckmann, G. S., Nehrke, G., Papadimitriou, S., Göttlicher, J., Steininger, R., Kennedy, H., Wolf-Gladrow, D., and Thomas, D.: Calcium carbonate as ikaite crystals in Antarctic sea ice, Geophys. Res. Lett., 35, L08501, https://doi.org/10.1029/2008gl033540, 2008.

Dieckmann, G. S., Nehrke, G., Uhlig, C., Göttlicher, J., Gerland, S., Granskog, M. A., and Thomas, D. N.: Brief Communication: Ikaite ($CaCO_3 \cdot 6H_2O$) discovered in Arctic sea ice, The Cryosphere, 4, 227–230, https://doi.org/10.5194/tc-4-227-2010, 2010.

Facchini, M. C., Rinaldi, M., Decesari, S., Carbone, C., Finessi, E., Mircea, M., Fuzzi, S., Ceburnis, D., Flanagan, R., Nilsson, E. D., de Leeuw, G., Martino, M., Woeltjen, J., and O'Dowd, C. D.: Primary submicron marine aerosol dominated by insoluble organic colloids and aggregates, Geophys. Res. Lett., 35, L17814, https://doi.org/10.1029/2008gl034210, 2008.

Gao, Q., Leck, C., Rauschenberg, C., and Matrai, P. A.: On the chemical dynamics of extracellular polysaccharides in the high Arctic surface microlayer, Ocean Sci., 8, 401–418, https://doi.org/10.5194/os-8-401-2012, 2012.

Gaston, C. J., Furutani, H., Guazzotti, S. A., Coffee, K. R., Bates, T. S., Quinn, P. K., Aluwihare, L. I., Mitchell, B. G., and Prather, K. A.: Unique ocean-derived particles serve as a proxy for changes in ocean chemistry, J. Geophys. Res.-Atmos., 116, D18310, https://doi.org/10.1029/2010jd015289, 2011.

Gross, D. S., Galli, M. E., Silva, P. J., and Prather, K. A.: Relative sensitivity factors for alkali metal and ammonium cations in single particle aerosol time-of-flight mass spectra, Anal. Chem., 72, 416–422, https://doi.org/10.1021/ac990434g, 2000.

Guasco, T. L., Cuadra-Rodriguez, L. A., Pedler, B. E., Ault, A. P., Collins, D. B., Zhao, D. F., Kim, M. J., Ruppel, M. J., Wilson, S. C., Pomeroy, R. S., Grassian, V. H., Azam, F., Bertram, T. H., and Prather, K. A.: Transition Metal Associations with Primary Biological Particles in Sea Spray Aerosol Generated in a Wave Channel, Environ. Sci. Technol., 48, 1324–1333, https://doi.org/10.1021/es403203d, 2014.

Hara, K., Osada, K., Yabuki, M., and Yamanouchi, T.: Seasonal variation of fractionated sea-salt particles on the Antarctic coast, Geophys. Res. Lett., 39, L18801, https://doi.org/10.1029/2012gl052761, 2012.

Keene, W. C., Maring, H., Maben, J. R., Kieber, D. J., Pszenny, A. A. P., Dahl, E. E., Izaguirre, M. A., Davis, A. J., Long, M. S., Zhou, X. L., Smoydzin, L., and Sander, R.: Chemical and physical characteristics of nascent aerosols produced by bursting bubbles at a model air-sea interface, J. Geophys. Res.-Atmos., 112, D21202, https://doi.org/10.1029/2007jd008464, 2007.

Kirpes, R. M., Bonanno, D., May, N. W., Fraund, M., Barget, A. J., Moffet, R. C., Ault, A. P., and Pratt, K. A.: Wintertime Arctic Sea Spray Aerosol Composition Controlled by Sea Ice Lead Microbiology, ACS Cent. Sci., 5, 1760–1767, https://doi.org/10.1021/acscentsci.9b00541, 2019.

Köllner, F., Schneider, J., Willis, M. D., Klimach, T., Helleis, F., Bozem, H., Kunkel, D., Hoor, P., Burkart, J., Leaitch, W. R., Aliabadi, A. A., Abbatt, J. P. D., Herber, A. B., and Borrmann, S.: Particulate trimethylamine in the summertime Canadian high Arctic lower troposphere, Atmos. Chem. Phys., 17, 13747–13766, https://doi.org/10.5194/acp-17-13747-2017, 2017.

Krembs, C., Eicken, H., Junge, K., and Deming, J. W.: High concentrations of exopolymeric substances in Arctic winter sea ice: implications for the polar ocean carbon cycle and cryoprotection of diatoms, Deep-Sea Res. Pt. I, 49, 2163–2181, https://doi.org/10.1016/S0967-0637(02)00122-X, 2002.

Krembs, C., Eicken, H., and Deming, J. W.: Exopolymer alteration of physical properties of sea ice and implications for ice habitability and biogeochemistry in a warmer Arctic, P. Natl. Acad. Sci. USA, 108, 3653–3658, https://doi.org/10.1073/pnas.1100701108, 2011.

Lawler, M. J., Saltzman, E. S., Karlsson, L., Zieger, P., Salter, M., Baccarini, A., Schmale, J., and Leck, C.: New Insights Into the Composition and Origins of Ultrafine Aerosol in the Summertime High Arctic, Geophys. Res. Lett., 48, e2021GL094395, https://doi.org/10.1029/2021gl094395, 2021.

Leck, C. and Bigg, E. K.: Source and evolution of the marine aerosol – A new perspective, Geophys. Res. Lett., 32, L19803, https://doi.org/10.1029/2005gl023651, 2005a.

Leck, C. and Bigg, E. K.: Biogenic particles in the surface microlayer and overlaying atmosphere in the central Arctic Ocean during summer, Tellus B, 57, 305–316, https://doi.org/10.1111/j.1600-0889.2005.00148.x, 2005b.

Leck, C. and Bigg, E. K.: New Particle Formation of Marine Biological Origin, Aerosol. Sci. Tech., 44, 570–577, https://doi.org/10.1080/02786826.2010.481222, 2010.

Leck, C. and Svensson, E.: Importance of aerosol composition and mixing state for cloud droplet activation over the Arctic pack ice in summer, Atmos. Chem. Phys., 15, 2545–2568, https://doi.org/10.5194/acp-15-2545-2015, 2015.

Leck, C., Gao, Q., Mashayekhy Rad, F., and Nilsson, U.: Size-resolved atmospheric particulate polysaccharides in the high summer Arctic, Atmos. Chem. Phys., 13, 12573–12588, https://doi.org/10.5194/acp-13-12573-2013, 2013.

Li, L., Huang, Z., Dong, J., Li, M., Gao, W., Nian, H., Fu, Z., Zhang, G., Bi, X., Cheng, P., and Zhou, Z.: Real time bipolar time-of-flight mass spectrometer for analyzing single aerosol particles, Int. J. Mass Spectrom., 303, 118–124, https://doi.org/10.1016/j.ijms.2011.01.017, 2011.

Liu, Z. M., Lu, X. H., Feng, J. L., Fan, Q. Z., Zhang, Y., and Yang, X.: Influence of Ship Emissions on Urban Air Quality: A Comprehensive Study Using Highly Time-Resolved Online Measurements and Numerical Simulation in Shanghai, Environ. Sci. Technol., 51, 202–211, https://doi.org/10.1021/acs.est.6b03834, 2017.

Mukherjee, P., Reinfelder, J. R., and Gao, Y.: Enrichment of calcium in sea spray aerosol in the Arc-

tic summer atmosphere, Mar. Chem., 227, 103898, https://doi.org/10.1016/j.marchem.2020.103898, 2020.

Murphy, D. M., Anderson, J. R., Quinn, P. K., McInnes, L. M., Brechtel, F. J., Kreidenweis, S. M., Middlebrook, A. M., Posfai, M., Thomson, D. S., and Buseck, P. R.: Influence of sea-salt on aerosol radiative properties in the Southern Ocean marine boundary layer, Nature, 392, 62–65, https://doi.org/10.1038/32138, 1998.

Norris, S. J., Brooks, I. M., de Leeuw, G., Sirevaag, A., Leck, C., Brooks, B. J., Birch, C. E., and Tjernström, M.: Measurements of bubble size spectra within leads in the Arctic summer pack ice, Ocean Sci., 7, 129–139, https://doi.org/10.5194/os-7-129-2011, 2011.

Oppo, C., Bellandi, S., Innocenti, N. D., Stortini, A. M., Loglio, G., Schiavuta, E., and Cini, R.: Surfactant components of marine organic matter as agents for biogeochemical fractionation and pollutant transport via marine aerosols, Mar. Chem., 63, 235–253, https://doi.org/10.1016/S0304-4203(98)00065-6, 1999.

Orellana, M. V. and Verdugo, P.: Ultraviolet radiation blocks the organic carbon exchange between the dissolved phase and the gel phase in the ocean, Limnol. Oceanogr., 48, 1618–1623, https://doi.org/10.4319/lo.2003.48.4.1618, 2003.

Orellana, M. V., Matrai, P. A., Leck, C., Rauschenberg, C. D., Lee, A. M., and Coz, E.: Marine microgels as a source of cloud condensation nuclei in the high Arctic, P. Natl. Acad. Sci. USA, 108, 13612–13617, https://doi.org/10.1073/pnas.1102457108, 2011.

Orellana, M. V., Hansell, D. A., Matrai, P. A., and Leck, C.: Marine Polymer-Gels' Relevance in the Atmosphere as Aerosols and CCN, Gels, 7, 185, https://doi.org/10.3390/gels7040185, 2021.

Passig, J., Schade, J., Irsig, R., Li, L., Li, X., Zhou, Z., Adam, T., and Zimmermann, R.: Detection of ship plumes from residual fuel operation in emission control areas using single-particle mass spectrometry, Atmos. Meas. Tech., 14, 4171–4185, https://doi.org/10.5194/amt-14-4171-2021, 2021.

Prather, K. A., Bertram, T. H., Grassian, V. H., Deane, G. B., Stokes, M. D., DeMott, P. J., Aluwihare, L. I., Palenik, B. P., Azam, F., Seinfeld, J. H., Moffet, R. C., Molina, M. J., Cappa, C. D., Geiger, F. M., Roberts, G. C., Russell, L. M., Ault, A. P., Baltrusaitis, J., Collins, D. B., Corrigan, C. E., Cuadra-Rodriguez, L. A., Ebben, C. J., Forestieri, S. D., Guasco, T. L., Hersey, S. P., Kim, M. J., Lambert, W. F., Modini, R. L., Mui, W., Pedler, B. E., Ruppel, M. J., Ryder, O. S., Schoepp, N. G., Sullivan, R. C., and Zhao, D. F.: Bringing the ocean into the laboratory to probe the chemical complexity of sea spray aerosol, P. Natl. Acad. Sci. USA, 110, 7550–7555, https://doi.org/10.1073/pnas.1300262110, 2013.

Pratt, K. A. and Prather, K. A.: Mass spectrometry of atmospheric aerosolsuRecent developments and applications. Part II: On-line mass spectrometry techniques, Mass. Spectrom. Rev., 31, 17–48, https://doi.org/10.1002/mas.20330, 2012.

Pratt, K. A., DeMott, P. J., French, J. R., Wang, Z., Westphal, D. L., Heymsfield, A. J., Twohy, C. H., Prenni, A. J., and Prather, K. A.: In situ detection of biological particles in cloud ice-crystals, Nat. Geosci., 2, 397–400, https://doi.org/10.1038/Ngeo521, 2009.

Qin, X. Y., Bhave, P. V., and Prather, K. A.: Comparison of two methods for obtaining quantitative mass concentrations from aerosol time-of-flight mass spectrometry measurements, Anal. Chem., 78, 6169–6178, https://doi.org/10.1021/ac060395q, 2006.

Quinn, P. K., Collins, D. B., Grassian, V. H., Prather, K. A., and Bates, T. S.: Chemistry and Related Properties of Freshly Emitted Sea Spray Aerosol, Chem. Rev., 115, 4383–4399, https://doi.org/10.1021/cr500713g, 2015.

Rankin, A. M., Wolff, E. W., and Martin, S.: Frost flowers: Implications for tropospheric chemistry and ice core interpretation, J. Geophys. Res.-Atmos., 107, AAC 4-1–AAC 4-15, https://doi.org/10.1029/2002jd002492, 2002.

Russell, L. M., Hawkins, L. N., Frossard, A. A., Quinn, P. K., and Bates, T. S.: Carbohydrate-like composition of submicron atmospheric particles and their production from ocean bubble bursting, P. Natl. Acad. Sci. USA, 107, 6652–6657, https://doi.org/10.1073/pnas.0908905107, 2010.

Salter, M. E., Hamacher-Barth, E., Leck, C., Werner, J., Johnson, C. M., Riipinen, I., Nilsson, E. D., and Zieger, P.: Calcium enrichment in sea spray aerosol particles, Geophys. Res. Lett., 43, 8277–8285, https://doi.org/10.1002/2016gl070275, 2016.

Schill, S. R., Collins, D. B., Lee, C., Morris, H. S., Novak, G. A., Prather, K. A., Quinn, P. K., Sultana, C. M., Tivanski, A. V., Zimmermann, K., Cappa, C. D., and Bertram, T. H.: The Impact of Aerosol Particle Mixing State on the Hygroscopicity of Sea Spray Aerosol, ACS Cent. Sci., 1, 132–141, https://doi.org/10.1021/acscentsci.5b00174, 2015.

Sierau, B., Chang, R. Y.-W., Leck, C., Paatero, J., and Lohmann, U.: Single-particle characterization of the high-Arctic summertime aerosol, Atmos. Chem. Phys., 14, 7409–7430, https://doi.org/10.5194/acp-14-7409-2014, 2014.

Sievering, H.: Aerosol non-sea-salt sulfate in the remote marine boundary layer under clear-sky and normal cloudiness conditions: Ocean-derived biogenic alkalinity enhances sea-salt sulfate production by ozone oxidation, J. Geophys. Res.-Atmos., 109, D19317, https://doi.org/10.1029/2003jd004315, 2004.

Song, C., Becagli, S., Beddows, D. C. S., Brean, J., Browse, J., Dai, Q., Dall'Osto, M., Ferracci, V., Harrison, R. M., Harris, N., Li, W., Jones, A. E., Kirchgäßner, A., Kramawijaya, A. G., Kurganskiy, A., Lupi, A., Mazzola, M., Severi, M., Traversi, R., and Shi, Z.: Understanding Sources and Drivers of Size-Resolved Aerosol in the High Arctic Islands of Svalbard Using a Receptor Model Coupled with Machine Learning, Environ. Sci. Technol., 56, 11189–11198, https://doi.org/10.1021/acs.est.1c07796, 2022.

Song, X. and Hopke, P. K.: Classification of single particles analyzed by ATOFMS using an artificial neural network, ART-2A, Anal. Chem., 71, 860–865, https://doi.org/10.1021/ac9809682, 1999.

Srivastava, A., Pitesky, M. E., Steele, P. T., Tobias, H. J., Fergenson, D. P., Horn, J. M., Russell, S. C., Czerwieniec, G. A., Lebrilla, C. S., Gard, E. E., and Frank, M.: Comprehensive assignment of mass spectral signatures from individual Bacillus atrophaeus spores in matrix-free laser desorption/ionization bioaerosol mass spectrometry, Anal. Chem., 77, 3315–3323, https://doi.org/10.1021/ac048298p, 2005.

Su, B., Wang, T., Zhang, G., Liang, Y., Lv, C., Hu, Y., Li, L., Zhou, Z., Wang, X., and Bi, X.: A review of atmospheric aging of sea spray aerosols: Potential factors affecting chloride depletion, Atmos. Environ., 290, 119365, https://doi.org/10.1016/j.atmosenv.2022.119365, 2022.

Su, B., Bi, X., and Zhang, G.: Enrichment of calcium in sea spray aerosol: Insights from bulk measurements and individual

particle analysis during the R/V Xuelong cruise in the summertime Ross Sea, Antarctica, Version 2, Zenodo [data set], https://doi.org/10.5281/zenodo.8279334, 2023.

Su, B. J., Zhuo, Z. M., Fu, Y. Z., Sun, W., Chen, Y., Du, X. B., Yang, Y. X., Wu, S., Xie, Q. H., Huang, F. G., Chen, D. H., Li, L., Zhang, G. H., Bi, X. H., and Zhou, Z.: Individual particle investigation on the chloride depletion of inland transported sea spray aerosols during East Asian summer monsoon, Sci. Total Environ., 765, 144290, https://doi.org/10.1016/j.scitotenv.2020.144290, 2021.

Sullivan, R. C., Moore, M. J. K., Petters, M. D., Kreidenweis, S. M., Roberts, G. C., and Prather, K. A.: Timescale for hygroscopic conversion of calcite mineral particles through heterogeneous reaction with nitric acid, Phys. Chem. Chem. Phys., 11, 7826–7837, https://doi.org/10.1039/b904217b, 2009.

Tobo, Y., Adachi, K., DeMott, P. J., Hill, T. C. J., Hamilton, D. S., Mahowald, N. M., Nagatsuka, N., Ohata, S., Uetake, J., Kondo, Y., and Koike, M.: Glacially sourced dust as a potentially significant source of ice nucleating particles, Nat. Geosci., 12, 253–258, https://doi.org/10.1038/s41561-019-0314-x, 2019.

Vancoppenolle, M., Meiners, K. M., Michel, C., Bopp, L., Brabant, F., Carnat, G., Delille, B., Lannuzel, D., Madec, G., Moreau, S., Tison, J.-L., and van der Merwe, P.: Role of sea ice in global biogeochemical cycles: emerging views and challenges, Quaternary Sci. Rev., 79, 207–230, https://doi.org/10.1016/j.quascirev.2013.04.011, 2013.

Verdugo, P.: Marine microgels, Annu. Rev. Mar. Sci., 4, 375–400, https://doi.org/10.1146/annurev-marine-120709-142759, 2012.

Verdugo, P., Alldredge, A. L., Azam, F., Kirchman, D. L., Passow, U., and Santschi, P. H.: The oceanic gel phase: a bridge in the DOM-POM continuum, Mar. Chem., 92, 67–85, https://doi.org/10.1016/j.marchem.2004.06.017, 2004.

Wang, Y. Q.: MeteoInfo: GIS software for meteorological data visualization and analysis, Meteorol. Appl., 21, 360–368, https://doi.org/10.1002/met.1345, 2014.

Wang, Y. Q., Zhang, X. Y., and Draxler, R. R.: TrajStat: GIS-based software that uses various trajectory statistical analysis methods to identify potential sources from long-term air pollution measurement data, Environ. Modell. Softw., 24, 938–939, https://doi.org/10.1016/j.envsoft.2009.01.004, 2009.

Willis, M. D., Leaitch, W. R., and Abbatt, J. P. D.: Processes Controlling the Composition and Abundance of Arctic Aerosol, Rev. Geophys., 56, 621–671, https://doi.org/10.1029/2018rg000602, 2018.

Wilson, T. W., Ladino, L. A., Alpert, P. A., Breckels, M. N., Brooks, I. M., Browse, J., Burrows, S. M., Carslaw, K. S., Huffman, J. A., Judd, C., Kilthau, W. P., Mason, R. H., McFiggans, G., Miller, L. A., Najera, J. J., Polishchuk, E., Rae, S., Schiller, C. L., Si, M., Temprado, J. V., Whale, T. F., Wong, J. P., Wurl, O., Yakobi-Hancock, J. D., Abbatt, J. P., Aller, J. Y., Bertram, A. K., Knopf, D. A., and Murray, B. J.: A marine biogenic source of atmospheric ice-nucleating particles, Nature, 525, 234–238, https://doi.org/10.1038/nature14986, 2015.

Yan, J., Jung, J., Zhang, M., Xu, S., Lin, Q., Zhao, S., and Chen, L.: Significant Underestimation of Gaseous Methanesulfonic Acid (MSA) over Southern Ocean, Environ. Sci. Technol., 53, 13064–13070, https://doi.org/10.1021/acs.est.9b05362, 2019.

Yan, J., Jung, J., Lin, Q., Zhang, M., Xu, S., and Zhao, S.: Effect of sea ice retreat on marine aerosol emissions in the Southern Ocean, Antarctica, Sci. Total Environ., 745, 140773, https://doi.org/10.1016/j.scitotenv.2020.140773, 2020a.

Yan, J., Jung, J., Zhang, M., Bianchi, F., Tham, Y. J., Xu, S., Lin, Q., Zhao, S., Li, L., and Chen, L.: Uptake selectivity of methanesulfonic acid (MSA) on fine particles over polynya regions of the Ross Sea, Antarctica, Atmos. Chem. Phys., 20, 3259–3271, https://doi.org/10.5194/acp-20-3259-2020, 2020b.

Yang, X., Pyle, J. A., and Cox, R. A.: Sea salt aerosol production and bromine release: Role of snow on sea ice, Geophys. Res. Lett., 35, L16815, https://doi.org/10.1029/2008gl034536, 2008.

Young, L.-H., Li, C.-H., Lin, M.-Y., Hwang, B.-F., Hsu, H.-T., Chen, Y.-C., Jung, C.-R., Chen, K.-C., Cheng, D.-H., Wang, V.-S., Chiang, H.-C., and Tsai, P.-J.: Field performance of a semi-continuous monitor for ambient $PM_{2.5}$ water-soluble inorganic ions and gases at a suburban site, Atmos. Environ., 144, 376–388, https://doi.org/10.1016/j.atmosenv.2016.08.062, 2016.

Zawadowicz, M. A., Froyd, K. D., Murphy, D. M., and Cziczo, D. J.: Improved identification of primary biological aerosol particles using single-particle mass spectrometry, Atmos. Chem. Phys., 17, 7193–7212, https://doi.org/10.5194/acp-17-7193-2017, 2017.

Zhang, T., Fiamingo, M., and Allen, H. C.: Trace Metal Enrichment Driven by Phosphate Functional Group Binding Selectivity, J. Geophys. Res.-Oceans, 123, 5286–5297, https://doi.org/10.1029/2018jc013926, 2018.